Recurrent liquefaction in Christchurch, New Zealand, during the Canterbury earthquake sequence

Mark C. Quigley[1], Sarah Bastin[1], and Brendon A. Bradley[2]
[1]Department of Geological Sciences, University of Canterbury, Christchurch 8014, New Zealand
[2]Department of Civil and Natural Resources Engineering, University of Canterbury, Christchurch 8014, New Zealand

ABSTRACT

Continuous observational monitoring of a study site in eastern Christchurch, New Zealand, following the 2010 M_w 7.1 Darfield earthquake has recorded ten distinct liquefaction episodes in the mainshock–aftershock sequence. Three nearby accelerometers allow calibration between the geological expressions of liquefaction and the intensity of earthquake-induced surface ground motion at the site. Sand blow formation was generated by M_w 5.2–7.1 earthquakes with M_w 7.5–normalized peak ground accelerations ($PGA_{7.5}$) of ≥ 0.057 g (acceleration due to gravity). Silt drapes between successive sand blow deposits provide markers for delineating distinct liquefaction-inducing earthquakes in the geologic record. However, erosion quickly modifies the surface of sand blows into alluvial and aeolian forms that complicate geologic diagnosis. The two feeder-dike generations identified in subsurface investigations significantly underrepresent the number of liquefaction-inducing earthquakes due to extensive dike reactivation. New constitutive equations enable $PGA_{7.5}$ variations to be estimated from the thickness and areal extent of sand blows.

INTRODUCTION

Cyclic shearing of loosely compacted, fluid-saturated sediments during earthquake-induced ground motion results in excess pore-water pressure and reduced shear strength in the affected media. Liquefaction occurs when excess pore pressures reach the initial vertical effective stress and is commonly accompanied by significant vertical (i.e., subsidence) and/or lateral (i.e., lateral spreading) ground movement. Liquefaction-induced ground deformation may result in severe infrastructure damage (e.g., Youd, 1986) and associated financial loss. Understanding the seismologic and geologic conditions under which liquefaction occurs and the preservation potential of liquefaction-induced features in the geological record are important for reducing societal vulnerability to earthquakes (e.g., Sims and Garvin, 1995; Green et al., 2005).

The ongoing Canterbury earthquake sequence (CES) in New Zealand's South Island includes the 4 September 2010 M_w 7.1 Darfield mainshock, and 45 $M_L \geq 5.0$ and 3 $M_L \geq 6.0$ subsequent aftershocks (Fig. 1A). The most damaging aftershock was the 22 February 2011 M_w 6.2 Christchurch earthquake that caused 185 fatalities. Land and infrastructure damage due to spatially extensive and recurrent liquefaction (Fig. 1B) resulted in a central government buyout of thousands of residential properties in eastern Christchurch at an estimated cost of over NZ$1 billion (http://www.stuff.co.nz/the-press/news/6489488/Red-zoned-homes-could-ve-been-saved). The lead author lived in one of these properties during the CES and photographically documented (Fig. 2) and mapped (Fig. 3) the areal extent of sand blows at this location following each successive liquefaction-inducing earthquake. Subsequent trenching investigations were conducted to reveal

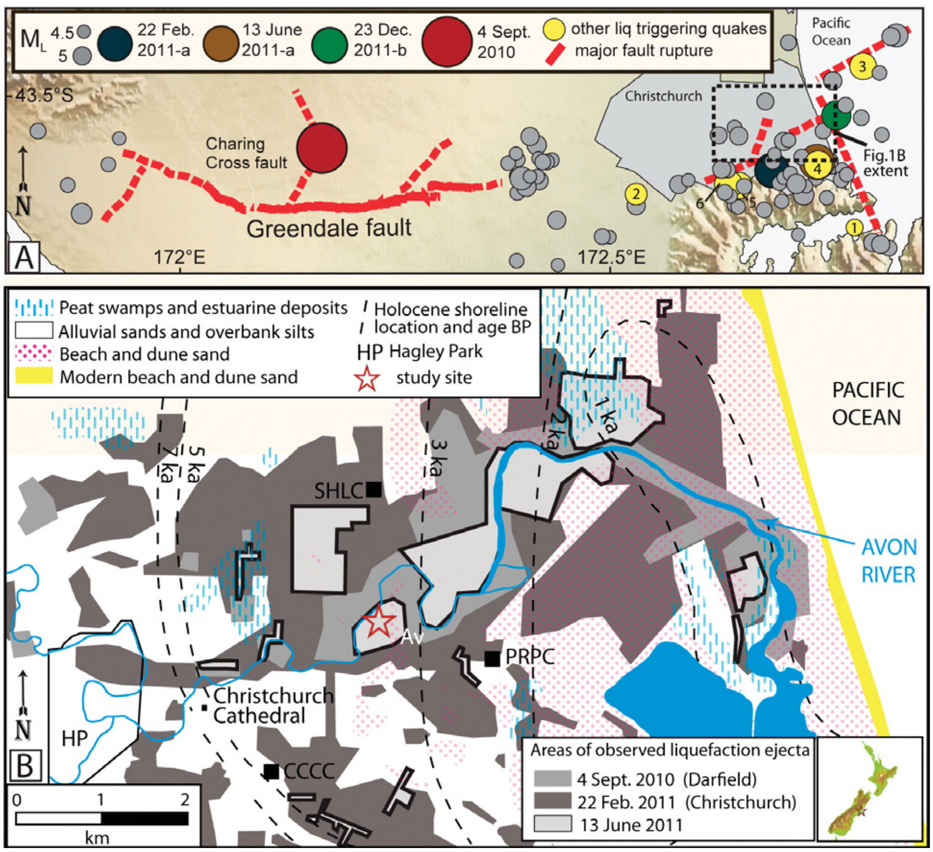

Figure 1. A: Epicentral locations of the Darfield earthquake (New Zealand) and Canterbury earthquake sequence (CES) aftershocks greater than M_L 4.5 (Bannister and Gledhill, 2012) that did (yellow, blue, brown, green, red) and did not (gray) generate liquefaction at the study site. Earthquakes: 1—16 April 2011; 2—21 June 2011; 3—23 December 2011-b; 4—13 June 2011-a; 5—22 February 2011-b; 6—22 February 2011-c. Darfield earthquake surface rupture on Greendale fault (bold red line) (Quigley et al., 2012) and projected locations (dashed red lines) of subsurface faults that ruptured in the Darfield, 22 February, 13 June, and 23 December 2011 earthquakes are shown (Beavan et al., 2012). liq—liquefaction. B: Areal extent of liquefaction in eastern Christchurch from the three largest earthquakes in the CES (Cubrinovski et al., 2012) overlain on simplified geological map (modified from Brown et al., 1995) showing approximate locations of Holocene sea levels (dashed lines with "ka" label denoting thousands of years before present [B.P.]). Location of strong ground motion seismometers (GeoNet stations) cited in this study (PRPC—Pages Road Pump Station; SHLC—Shirley Boys High School; CCCC—Christchurch Cathedral Grammar School), Christchurch Cathedral (located in central business district), and Hagley Park (HP) are shown.

GEOLOGY, April 2013; v. 41; no. 4; p. 419–422; Data Repository item 2013113 | doi:10.1130/G33944.1 | Published online 7 February 2013

Figure 2. A–F: Field photographs (looking southwest) of sand blows at study site following the (A) Darfield M_L 7.1 earthquake, (B) 22 February 2011 M_L 6.3, 5.8, and 5.9 earthquakes, (C) 16 April 2011 M_L 5.5 earthquake, (D) 13 June 2011-a M_L 5.6 earthquake, (E) 13 June 2011-b M_L 6.4 earthquake, and (F) 23 December 2011 M_L 5.8 and 6.0 earthquakes. All photos were taken from same location within 3 h of last inducing earthquake. G: Distinct liquefaction ejecta units in sand blow stratigraphy. Arrows and nails denote silt drapes. Cross-bedding as sketched. Location of photographed portion of trench location shown in F. H: Microrill development in silt drape at edge of a sand blow. I: Post-depositional erosion of sand blow and silt drape to form parabolic microdunes and ripples only 2 mo after formation.

the subsurface architecture of sand blows and feeder-dike systems (Figs. DR1 and DR2 in the GSA Data Repository[1]). In this paper, detailed geologic investigations are combined with proximally derived strong ground motion data to infer the approximate liquefaction-triggering threshold and geological controls on the surface manifestation of liquefaction at the study site. These data are further used to investigate the feasibility of obtaining robust seismologic information from the geologic record of paleoliquefaction.

GEOLOGIC AND SEISMOLOGIC SETTING

The city of Christchurch (population 360,000) is predominantly located on a low-relief, low-elevation (0–20 m above sea level [asl]) alluvial landscape (Fig. 1A). Much of the central and eastern city is built upon alluvial silt and sand deposits, drained peat swamps and estuaries, sand of stable to semistable dunes, and underlying marine sands (collectively referred to as the Christchurch Formation) that formed as sea levels transgressed then regressed from a mid-Holocene highstand that reached to ~1 km west of Hagley Park at 6.5 ka (Fig. 1B) (Brown et al., 1995). High water tables (typically 1–2 m depth) and the loosely consolidated nature of Holocene fine-grained sands and non- and low-plastic silts limit soil cementation and aging effects. These sediments pose a long-recognized liquefaction hazard for Christchurch (Elder et al., 1992) that was dramatically confirmed during the CES (Fig. 1B) (Cubrinovski et al., 2012).

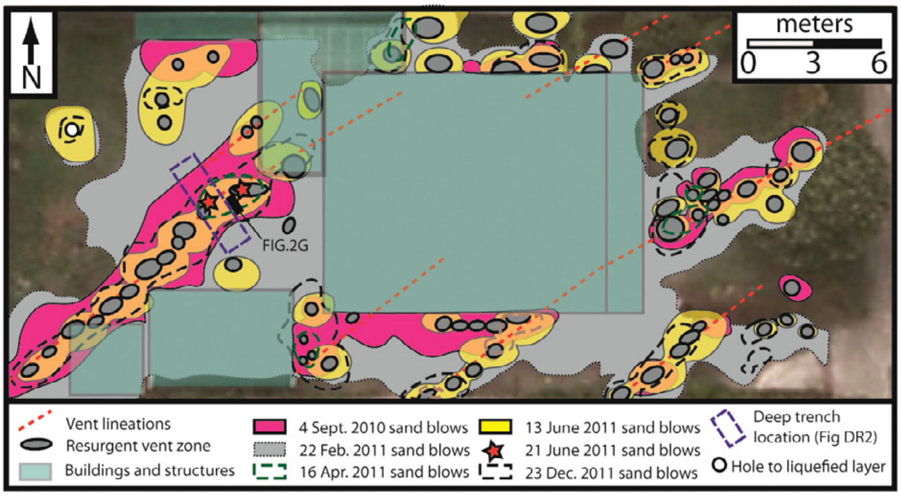

Figure 3. Detailed map of sand blows and source vents at study site for liquefaction-inducing Canterbury earthquake sequence (CES) events. Mapped extents reflect cumulative sediment deposition from multiple events for the 22 February, 13 June, and 23 December 2011 earthquakes. Areal extents in square meters and as a percent of total study site area are Darfield (65 m^2; 12%), 22 February (344 m^2; 64%), 16 April (6 m^2; 1%),) 13 June (78 m^2; 14%), 21 June (1 m^2; <1%), and 23 December (43 m^2; 8%). Fig. DR2 is Figure DR2 in the Data Repository (see footnote 1).

At least five earthquakes since A.D. 1869 have generated Modified Mercalli Intensities (MMIs) ≥6 in central Christchurch (Downes and Yetton, 2012). The CES initiated with the rupture of at least seven distinct faults in the Charing Cross–Greendale fault system during the Darfield earthquake (Fig. 1A) (Beavan et al., 2012; Quigley et al., 2012). An energetic aftershock sequence including the 22 February 2011 earthquake cluster (M_L 6.3, 5.8, and 5.9 earthquakes within 2 h), the 13 June earthquake cluster (M_L 5.6 and 6.4 earthquakes within 1 h 20 min), and the 23 December earthquake cluster (M_L 5.8 and 6.0 within 1 h 20 min) followed (Fig. 1A).

METHODS

The study site is located at 11 Bracken Street, Avonside, in eastern Christchurch, within

[1]GSA Data Repository item 2013113, Christchurch liquefaction mapping and seismologic data, is available online at www.geosociety.org/pubs/ft2013.htm, or on request from editing@geosociety.org or Documents Secretary, GSA, P.O. Box 9140, Boulder, CO 80301, USA.

overbank silt and fine-grained sand surface deposits (Fig. 1B). The residential dwelling at the study site was occupied by the lead author through the CES until August 2011, and subsequently revisited following aftershocks with recorded peak ground accelerations (PGAs) of ≥0.1 g on local accelerometers. New sand blows were identified and photographed (Fig. 2) within 3 h of individual earthquakes or earthquake clusters. The study site was cleaned of any liquefaction ejecta after the Darfield, 22 February 2011, and 16 April earthquakes, so that observed sand blow accumulations record these events only. However, the site was left undisturbed following the 13 June earthquakes; thus sand blows deposited after this event were deposited onto previous blows. Residents living in the area observed three distinct sand blow depositional events during the 22 February earthquake sequence and two pulses in the 23 December sequence, consistent with instrumental records of several strong ground motion events with PGA in excess of 0.2 g (Table DR1 in the Data Repository); however, photographs of the study site were acquired only following the last event. Sand blows were rapidly photographed for both earthquakes in the 13 June sequence despite a lapse time of only 1 h 20 m between these events (Figs. 2D and 2E).

Field mapping of sand blows and vents was undertaken within 2–3 d of the associated earthquake (sequence) (Fig. 3), and maps were further refined using field photographs and post-earthquake aerial photography for the Darfield earthquake and the 22 February earthquake (aerial photography for the study site following the Darfield earthquake was obtained by GeoEye on 4 September 2010 [New Zealand Standard Time {NZST}], and is viewable through Google Earth™ [http://www.googleearth.com]; aerial photography for the Christchurch earthquake, flown on 24 February 2011 [NZST] by NZ Aerial Mapping for the Christchurch Response Centre, is available at http://koordinates.com/layer/3185-christchurch-post-earthquake-aerial-photos-24-feb-2011/). Areal extent (*AE*) of sand blows was calculated from mapped extents using ArcGIS (http://www.esri.com/software/arcgis). Shallow trenches (~20 cm deep) were excavated through sand blows in April 2012 in order to characterize the sand blow stratigraphy and maximum stratigraphic thicknesses (*ST*) developed from the 13 June and 23 December events. *ST* for prior events was estimated from maps and photographs. An ~1.2-m-deep trench (see Fig. 3 for location) was excavated perpendicular to the linear vent zone in Figure 2 to investigate the cumulative geologic expression of all CES earthquakes in the sand blow–feeder dike system (Fig. DR2).

Strong-ground-motion data for 38 M_w ≥4.5 earthquakes was obtained from accelerometers at distances of 1.61 km (GeoNet station PRPC), 1.78 km (station SHLC), and 2.33 km (station CCCC) from the study site using the GeoNet Strong Ground Motion database (http://info.geonet.org.nz/display/appdata/Strong-Motion+Data) (Fig. 1B). Recorded two-component PGAs were linearly interpolated for the study site using distance-weighted averaging and converted to geometric mean PGAs. The effect of shaking duration and frequency content were accounted for using a magnitude scaling factor, MSF. The equivalent PGA for a M_w 7.5 event ($PGA_{7.5}$ = PGA × 1 / MSF) was computed, which is directly proportional to the peak shear stress induced in the soil deposit (Youd et al., 2001). Cumulative $PGA_{7.5}$ values were determined for M_w >5 earthquakes that occurred within 1–3 h of temporally adjacent events assuming no drainage as sand blow formation is likely to have occurred in each of these events. $PGA_{7.5}$ is plotted against earthquake M_w for liquefaction-inducing events (Fig. 4A). Individual or cumulative $PGA_{7.5}$ is plotted against *AE* and *ST* to derive constitutive equations for the study site that may also apply to sites with similar geotechnical properties (Fig. DR4). *AE*, *ST*, and $PGA_{7.5}$ were normalized against maximum *AE*, *ST*, and $PGA_{7.5}$ values recorded in the 22 February earthquake to produce constitutive equations to compare relative changes in *AE* and *ST* (*AE**, *ST**) to relative changes in $PGA_{7.5}$ ($PGA_{7.5}$*) (Fig. 4B). Seismologic (Table DR1) and geotechnical data (Figs. DR4 and DR5) for the study site are available in the Data Repository.

RESULTS AND DISCUSSION

Seven distinct episodes of earthquake-induced sand blow deposition were photographed and mapped at the study site, and an additional three episodes were inferred after corroboration between the observations of local residents and the instrumental record (Fig. 4A; Table DR1). Although compound sand blows and feeder dikes have been recognized and attributed to closely timed earthquakes in earthquake sequences (Sims and Garvin, 1995; Tuttle et al., 2002), documentation of recurrent liquefaction to this detail and extent, including the recording of ten distinct liquefaction-related sedimentation events during a single mainshock–aftershock sequence, is unprecedented.

Mapped vent distributions reveal persistent reactivation along distinct northeast-oriented alignments (Figs. 2 and 3) that are subparallel to the closest section of the Avon River ~120 m to the northwest of the study site (Fig. 1B). This indicates that near-surface cracking and sand blow venting occurred perpendicular to the direction of lateral spreading toward the closest "free face" at the river bank edge, with transport facilitated by basal glide within the liquefiable layer at depths of 2–5 m (Figs. DR2 and DR4). Vent zones established in the Darfield earthquake were repeatedly reactivated in successive events with exception of a small sand blow in the northwest corner of the study site (Fig. 3). This location showed no evidence for sand blow deposition after the Darfield earthquake, at which time a small (~10 cm diameter) hole was cored to depths of ~2 m, where the liquefiable layer was encountered. This hole gradually closed at the surface prior to the Christchurch earthquake, but erupted as a source conduit for sand blow formation in the 22 February, 13 June, and 23 December earthquakes, with the highest observed sediment flux rate on site in the 13 June earthquakes (Video DR1 in the Data Repository). This confirms that preexisting zones of weakness in the near surface (e.g., higher-permeability fracture

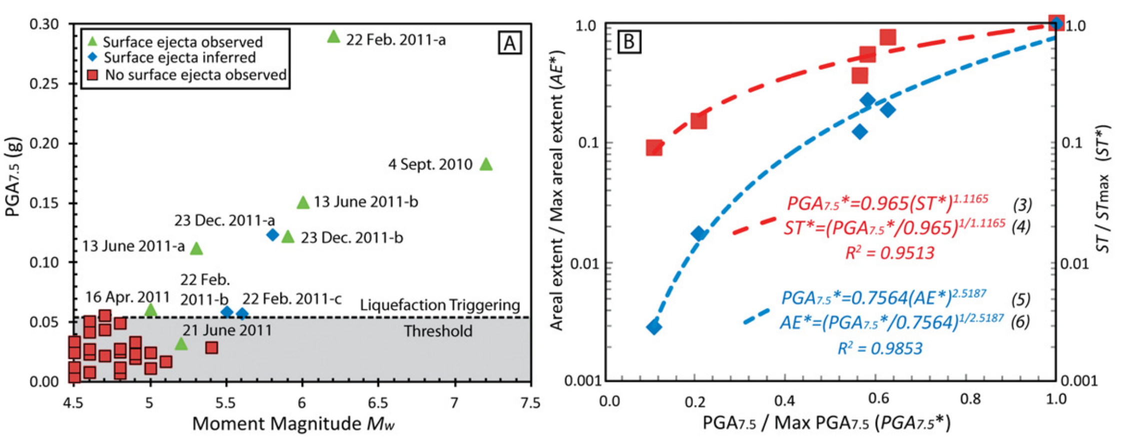

Figure 4. A: Peak ground acceleration normalized to M_w 7.5 earthquake ($PGA_{7.5}$) versus M_w and relationship to approximate liquefaction-triggering threshold for selected M_w ≥4.5 earthquakes. Liquefaction-triggering threshold of 0.056 g $PGA_{7.5}$ is shown. B: Sand blow areal extent (*AE*), maximum stratigraphic thickness (*ST*), and $PGA_{7.5}$ normalized to 22 February 2011 earthquake maxima (*AE, *ST**, $PGA_{7.5}$*), and corresponding power-law Equations 3–6.**

zones or conduits through otherwise low-permeability layers overlying the liquefiable layer) exert a first-order control on the vent distribution of sand blows by providing more-efficient pathways for liquefied material to move vertically.

The liquefaction limit, as defined by the minimum $PGA_{7.5}$ threshold for sand blow formation, at the site is ~0.057 g (Fig. 4A). The highest recorded $PGA_{7.5}$ without surface expression of liquefaction was the 25 December 2010 earthquake with $PGA_{7.5}$ of 0.056 g. An isolated small (<1 m^2) sand blow was observed following the 21 June 2011 earthquake at a $PGA_{7.5}$ of 0.032 g, well below the proposed threshold. The water table at the study site (~1 m depth) is at a similar elevation to the Avon River, which undergoes minor (<50 cm) tidal fluctuations at this location. We thus infer that major changes in groundwater tables from earthquake to earthquake are unlikely and that the liquefiable layer remains saturated regardless of seasonal conditions. However, it is possible that temporarily high winter water tables after extensive rainfall and/or the close timing (~1 week) between the 21 June and the 13 June 2011 earthquake sequences may have resulted in formation of a shallow-water interlayer within pockets of shallower liquefiable sediment that was remobilized in this earthquake despite a below-threshold $PGA_{7.5}$. The lack of surface liquefaction ejecta in the 25 December 2010 earthquake could conversely be attributed to slightly lower summer water tables and/or a relatively longer lapse time between the previous liquefaction-inducing earthquake (~4 mo). Clearly these factors are only relevant at near-threshold $PGA_{7.5}$ values, as indicated from the pronounced liquefaction in the Christchurch and 23 December 2011 earthquakes that occurred under similar (summer) weather conditions.

Shallow trenching of a sand blow where four sand blow depositional events were observed (Figs. 2D–2F; Fig. DR1) reveals four distinct fine-sand ejecta units that each grade from a reddish-colored, oxidized basal sand to a lighter-gray, clean, fine-grained sand capped by a thin (<0.5 cm) coarse-silt to very-fine-sand drape (Fig. 2G) that formed from suspended sediment as ejected groundwater drained following the liquefaction event (Fig. 2E; Video DR1). The top layer (23 December 2011-b) contains evidence for erosion and sediment remobilization such as postdepositional channel formation on sand blow flanks (Fig. 2F), cross-bed sets in remobilized deposits near ejecta packet tops (Fig. 2G), and microrilling (Fig. 2H). After 2.5 mo, significant erosion of sand blow features was observed, including vent degradation, crusting and breakup of the silt drape, and formation of ripples and parabolic microdunes (Fig. 2I). Deeper trenching of the feeder dike system to >1 m depth (Fig. DR2) reveals only one clear crosscutting relationship (two discernible dike generations) despite at least eight liquefaction events sourced through this system. Our observations indicate that sand blow sequences can provide robust geologic archives of successive liquefaction-inducing earthquakes, particularly where capping silt drapes are well preserved (e.g., Tuttle et al., 2002). Because surface features may erode into alluvial and aeolian forms rapidly (e.g., weeks to months), silt drapes that aid in distinguishing different sand blow pulses are more likely to be preserved during temporally clustered earthquake sequences (e.g., mainshock–aftershock or otherwise triggered events over months to years) rather than recurring mainshocks on the same fault (return times of ~10^2–10^5 yr). The number of distinguishable feeder dike generations should be treated as an absolute minimum estimate of, and may significantly underrepresent, the number of liquefaction-inducing earthquakes at a given site (e.g., Sims and Garvin, 1995).

AE and *ST* positively co-vary with $PGA_{7.5}$ (or cumulative $PGA_{7.5}$ for clustered events) (Fig. DR6) with statistical best fit defined by power-law equations,

$$PGA_{7.5} = 5773.2 \times AE^{2.5187} \ (R^2 = 0.9853) \quad (1)$$

$$PGA_{7.5} = 125.87 \times ST^{1.1165} \ (R^2 = 0.9513). \quad (2)$$

Equations 1 and 2 enable $PGA_{7.5}$ to be estimated from paleoseismic mapping of sand blow *AE* and *ST*, and/or *AE* and *ST* to be predicted for future earthquakes of given $PGA_{7.5}$ for this and other sites with comparable geologic, hydrologic, and geotechnical characteristics. By normalizing the values from the smaller CES events to the maximums associated with the 22 February 2011 event, we derive new constitutive power-law equations of relative *AE* and *ST* variations as a function of relative $PGA_{7.5}$ variations (Equations 3–6 in Fig. 4B). Where compound sand blow sequences are identified in the geologic record, these equations enable the characterization of relative $PGA_{7.5}$ values in the absence of any major interevent changes to liquefaction susceptibility. Any changes in the sedimentary layer that liquefied in this instance do not appear to have influenced the liquefaction susceptibility during the CES. This empirical data set provides information relevant to paleoliquefaction studies, liquefaction susceptibility modeling, and land-use planning in New Zealand and elsewhere.

ACKNOWLEDGMENTS

We thank M. Tuttle, K. Bassett, R. Green, P. Villamor, J. Begg, and M. Cubrinovski for insightful scientific discussions, and B. Mackey for conducting sand blow area calculations. This work was funded by New Zealand's Earthquake Commission.

REFERENCES CITED

Bannister, S., and Gledhill, K., 2012, Evolution of the 2010–2012 Canterbury earthquake sequence: New Zealand Journal of Geology and Geophysics, v. 55, p. 295–304, doi:10.1080/00288306.2012.680475.

Beavan, J., Motagh, M., Fielding, E., Donnelly, N., and Collett, D., 2012, Fault slip models of the 2010–2011 Canterbury, New Zealand, earthquakes from geodetic data, and observations of post-seismic ground deformation: New Zealand Journal of Geology and Geophysics, v. 55, p. 207–221, doi:10.1080/00288306.2012.697472.

Brown, L.J., Beetham, R.D., Paterson, B.R., and Weeber, J.H., 1995, Geology of Christchurch, New Zealand: Environmental & Engineering Geoscience, v. 1, p. 427–488.

Cubrinovski, M., and McCahon, I., 2011, Foundations on Deep Alluvial Soils: Christchurch, New Zealand, University of Canterbury, technical report prepared for the Canterbury Earthquakes Royal Commission, 40 p.

Cubrinovski, M., Robinson, K., Taylor, M., Hughes, M., and Orense, R., 2012, Lateral spreading and its impacts in urban areas in the 2010–2011 Christchurch earthquakes: New Zealand Journal of Geology and Geophysics, v. 55, p. 255–269, doi:10.1080/00288306.2012.699895.

Downes, and Yetton, M., 2012, Pre-2010 historical seismicity near Christchurch, New Zealand: The 1869 M_W 4.7–4.9 Christchurch and 1870 M_W 5.6–5.8 Lake Ellesmere earthquakes: New Zealand Journal of Geology and Geophysics, v. 55, p. 199–205.

Elder, D.M.G., McCahon, I.F., and Yetton, M., 1992, The Earthquake Hazard in Christchurch: A Detailed Evaluation: New Zealand Earthquake Commission (EQC) Research Paper No. 105, 131 p.

Green, R.A., Obermeier, S.F., and Olson, S.M., 2005, Engineering geologic and geotechnical analysis of paleoseismic shaking using liquefaction effects: Field examples: Engineering Geology, v. 76, p. 263–293, doi:10.1016/j.enggeo.2004.07.026.

Quigley, M., Van Dissen, R., Litchfield, N., Villamor, P., Duffy, B., Barrell, D., Furlong, K., Stahl, T., Bilderback, E., and Noble, E., 2012, Surface rupture during the 2010 M_W 7.1 Darfield (Canterbury) earthquake: Implications for fault rupture dynamics and seismic-hazard analysis: Geology, v. 40, p. 55–58, doi:10.1130/G32528.1.

Sims, J.D., and Garvin, C.D., 1995, Recurrent liquefaction induced by the 1989 Loma Prieta earthquake and 1990 and 1991 aftershocks: Implications for paleoseismicity studies: Bulletin of the Seismological Society of America, v. 85, p. 51–65.

Tuttle, M.P., Schweig, E.S., Sims, J.D., Lafferty, R.H., Wolf, L.W., and Haynes, M.L., 2002, The earthquake potential of the New Madrid seismic zone: Bulletin of the Seismological Society of America, v. 92, p. 2080–2089, doi:10.1785/0120010227.

Youd, L.T., 1986, Major cause of earthquake damage is ground failure: Civil Engineering (American Society of Civil Engineers), v. 48, no. 4, p. 47–51.

Youd, T.L., and 20 others, 2001, Liquefaction resistance of soils: Summary report from the 1996 NCEER and 1998 NCEER/NSF workshops on evaluation of liquefaction resistance of soils: Journal of Geotechnical and Geoenvironmental Engineering, v. 127, p. 817–833, doi:10.1061/(ASCE)1090-0241(2001)127:10(817).

Manuscript received 13 August 2012
Revised manuscript received 16 October 2012
Manuscript accepted 17 October 2012

Printed in USA